# ESTIMATING ROCK AND SLAG WOOL FIBER DISSOLUTION RATE FROM COMPOSITION

*Walter Eastes, Russell M. Potter, and John G. Hadley*

Owens Corning, Science and Technology Center, Granville, Ohio, USA

Originally published:
*Inhalation Toxicology*, in press (2000)



## ABSTRACT

A method was tested for calculating the dissolution rate constant in the lung for a wide variety of synthetic vitreous silicate fibers from the oxide composition in weight percent. It is based upon expressing the logarithm of the dissolution rate as a linear function of the composition and using a different set of coefficients for different types of fibers. The method was applied to 29 fiber compositions including rock and slag fibers as well as refractory ceramic and special purpose, thin E glass fibers and borosilicate glass fibers for which in-vivo measurements have been carried out. These fibers had dissolution rates that ranged over a factor of about 400, and the calculated dissolution rates agreed with the in-vivo values typically within a factor of four. The method presented here is similar to one developed previously for borosilicate glass fibers that was accurate to a factor of 1.25. The present coefficients work over a much broader range of composition than the borosilicate ones but with less accuracy. The dissolution rate constant of a fiber may be used to estimate whether disease would occur in animal inhalation or intraperitoneal injection studies of that fiber.

## INTRODUCTION

The main property that determines the results of animal studies of different types of fibers, tested at the same dose of the same length and diameter, is the dissolution rate constant of the long fibers in the extracellular environment of the lung (Eastes and Hadley, 1996). This paper describes a reasonably accurate and efficient method for computing this dissolution rate constant directly from the oxide composition for a wide range of rock and slag wool compositions. The compositions for which this method works cover the range of both high alumina new rock wools and conventional low alumina rock wool compositions, many slag wools, as well as a variety of other synthetic vitreous silicate fiber compositions.

The dissolution rate constant has been shown to predict the decrease in diameter of long fibers after intratracheal instillation in rats (Eastes et al., 1995), and to predict the biopersistence of long fibers after short-term inhalation in rats (Bernstein et al., 1996; Eastes and Hadley, 1995). Additionally, the dissolution rate constant can be used to predict the incidence of fibrosis and lung tumors following inhalation and tumors following intraperitoneal injection in rats (Eastes and Hadley, 1996). It may also be measured accurately in many cases in vitro (Potter and Mattson, 1991; Mattson, 1994) and a standard protocol is available for performing these measurements (Bauer et al., 1997).

The dissolution rate constant $k_{dis}$ is an expression of the rate at which a fiber, particularly one longer than 10 to 20 $\mu$m or too long to be effectively enveloped by alveolar macrophages, dissolves in the mammalian lung and is eliminated thereby. The complete disappearance of the long fiber from the lung may take place by total dissolution and systemic removal of the dissolution products, by breakage of the partially leached fiber and macrophage mediated clearance of the fragments, or by a combination of these mechanisms. The exact extent and contribution of each of these mechanisms is not so important as the fact that they both occur because of dissolution, which is captured in the $k_{dis}$ parameter.

The next section describes the theory involved in obtaining an expression for the dissolution rate constant of a fiber from its composition. The following section applies the theory to a set of fiber compositions for which reliable dissolution rates are available from in-vivo inhalation biopersistence studies. The final section discusses the implications of these results.

## THEORY

The dissolution rate of a fiber is approximated here as proportional to its surface area. The dissolution is thus considered to be a zero order reaction (Scholze, 1988), in the sense that it is independent of reactant concentrations. The dissolution rate is proportional to the fiber surface area, which changes with time as it dissolves, and to the dissolution rate constant $k_{dis}$. The parameter $k_{dis}$ in this reaction is a property of the material making up the fiber, and does not depend on its size or shape. Thus $k_{dis}$ depends on the fiber composition, conventionally expressed as the weight percent of oxides. One may expect, therefore, to be able to calculate $k_{dis}$ to a reasonable approximation directly from the oxide composition. The $k_{dis}$ depends also, but to a much lesser extent for most fibers, on the glass structure that is affected by the fiber cooling rate and thus by the method of fiberizing and the fiber diameter (Potter and Mattson, 1991; Scholze, 1988). These effects are much smaller than the influence of composition on $k_{dis}$. Often they are so small as to be unobservable (Scholze, 1988), and they will not be considered in what follows.

The theory of calculating fiber dissolution from composition has been described in detail previously (Eastes et al., 2000a). Briefly, it consists of the observation that, by virtue of the Arrhenius rate equation, the logarithm of $k_{dis}$ is approximately proportional to a weighted sum of the oxide weight percents:

$$\log k_{dis} = \sum_{i=1}^{n} P_i W_i \qquad \textbf{(1)}$$

Each $W_i$ is the weight percent of oxide $i$ for $i = 1$ through $n$ oxides and each $P_i$ is the coefficient of the corresponding $W_i$. These coefficients are found most conveniently by fitting measured $k_{dis}$ values for fibers of known composition to Eq. (1) in the minimum $\chi^2$ sense. While the Arrhenius rate equation applied here is most often used to relate reaction rate to temperature, it also involves the reaction activation energy. The Arrhenius rate equation is used here at constant body temperature to describe the relation between dissolution rate and the activation energy, which is approximately expressed in Eq. (1).

In a previous publication (Eastes et al., 2000a), this procedure was carried out for a large set of borosilicate glass wool fibers with in-vitro measured $k_{dis}$ values. It was found that a single set of coefficients $P_i$ in Eq. (1) fit the measured $k_{dis}$ reasonably well over a fairly wide range of compositions. However, it would be expected that neither the previous coefficients $P_i$ nor any single set of coefficients would fit adequately all of the rock and slag wool fiber compositions for at least two reasons: First, the rock and slag compositions contain no boron and have mostly lower silica ($SiO_2$) concentrations than the borosilicate glass wool fibers. These facts suggest that the nature of the glass forming network would be different and that at least the coefficient for silica in Eq (1) would be different. Second, the alumina ($Al_2O_3$) concentration in the rock and slag wools ranges from nearly 0 to 50% by weight, with the larger concentrations represented by the newer, high-alumina rock wool fibers, whereas the range was only 0 to 7.5% in the borosilicate fibers. It would not be unexpected for the structure of aluminum in the glass network to be qualitatively different at the lower alumina concentrations than at the higher ones, leading to different coefficients $P_i$ for alumina at lower concentrations than at higher weight percent. On the other hand, it might be expected that the other components of the rock and slag fibers, the network modifiers like CaO, MgO, and $Na_2O$, would act similarly in the rock and slag fibers as they do in the borosilicates, because they tend to disrupt the silicate network that is present in all of these silicate fibers.

If these suggestions about the effect of different components of the rock and slag fibers on $k_{dis}$ are correct, then all of the coefficients $P_i$ in Eq. (1) except those for silica and alumina can be taken to be the same as for the borosilicate glass fibers. Then Eq (1) may be partitioned

$$\log k_{dis} = P_{SiO_2} W_{SiO_2} + P_{Al_2O_3} W_{Al_2O_3} + \sum_{i=3}^{n} P_i W_i, \quad \textbf{(2)}$$

in which the sum is over all oxides except silica and alumina. For fibers of known composition for which $k_{dis}$ has been measured, a temporary new quantity, the "partial dissolution rate" $S$, may be defined by a rearrangement of Eq (2):

$$S = \frac{\log k_{dis} - \sum_{i=3}^{n} P_i W_i}{W_{SiO_2}} = P_{SiO_2} + P_{Al_2O_3} \frac{W_{Al_2O_3}}{W_{SiO_2}} \quad \textbf{(3)}$$

The partial dissolution rate $S$ in Eq (3) is seen to be a linear function of the $Al_2O_3/SiO_2$ weight ratio. The extent to which Eq (3) holds and the range of compositions over which $S$ is linear with the same coefficients may be determined by computing S for a series of compositions for which $k_{dis}$ is known and plotting it as a function of the weight ratio.

If these considerations are shown to be generally correct by a demonstration that the partial dissolution rate $S$ is approximately linear in the alumina/silica ratio, then it is feasible to take the method one step further. One or more other oxides could be split out of the sum in Eq. (2) of those oxides for which coefficients $P_i$ are available and fit to the measured dissolution rate. One good candidate for such an oxide is FeO. Only a small amount of iron oxide is present in the borosilicate glass fibers considered previously, and much of that is in the $Fe_2O_3$ oxidation state, since these glasses are melted under oxidizing conditions. Many rock wool compositions, on the other hand, contain ten times as much iron oxide and much of that is in the FeO state due to the reducing conditions in these furnaces. Thus it is reasonable to fit FeO for these compositions to an equation of the form

$$\log k_{dis} = P_{SiO_2} W_{SiO_2} + P_{Al_2O_3} W_{Al_2O_3} + P_{FeO} W_{FeO} + \sum_{i=4}^{n} P_i W_i. \quad \textbf{(4)}$$

A determination of the coefficients $P_{SiO_2}$, $P_{Al_3O_3}$, and $P_{FeO}$ involves fitting the measured $k_{dis}$ and composition data to Eq (4). An important detail in these fits is to normalize the composition of each fiber to 100% in all of the oxides included in the fit (Eastes et al., 2000a).

---

**Table 1.** Animal studies used to obtain in-vivo $k_{dis}$ values to fit to composition data.

| Fibers | Study Type | Reference |
|---|---|---|
| 7753, 7484, 7779, MMVF 10, MMVF 11 | Intratracheal Instillation | Eastes et al., 1995 |
| RCF 1a, Rock MMVF 21, E MMVF 32, JM475 MMVF 33, and HT MMVF 34 | Short-term Inhalation | Hesterberg et al., 1998 |
| SG MMVF 11, SG A, SG B, SG C, SG F, SG G, SG H, SG J X607, and SG L | Short-term Inhalation | Bernstein et al., 1996 |
| JM 901 MMVF 10, CT B MMVF 11, Rock Wool MMVF 21, and Slag Wool MMVF 22 | Short-term Inhalation | Musselman et al., 1994 |

## RESULTS

A number of in-vivo measurements of rock and slag wool fiber dissolution rate constants $k_{dis}$ have been made on fibers with known compositions that allow one to test the theory just described, and these are summarized in Table 1. Two separate biopersistence studies have been done on a conventional rock wool composition known as MMVF 21 (Musselman et al., 1994; Hesterberg et al., 1998), and the in-vivo $k_{dis}$ has been obtained from each study (Eastes et al., 2000b). These in-vivo $k_{dis}$ values agree well with each other and with the in-vitro measured values. These in-vivo $k_{dis}$ values also agree well with that for a similar composition, SG L (Bernstein et al., 1996). A slag wool denoted MMVF 22 was also tested for biopersistence (Musselman et al., 1994). A biopersistence study of two low alumina rock wool compositions with high dissolution rates has also been reported (Bernstein et al., 1996). An extreme example of a high alumina fiber, a refractory ceramic fiber denoted RCF 1a, was also the subject of a biopersistence study (Hesterberg et al., 1998). Finally, a series of high alumina rock wool compositions were tested in biopersistence studies (Hesterberg et al., 1998; Eastes et al., 2000b).

The in-vivo dissolution rate constant $k_{dis}$ has been calculated (Eastes et al., 2000b) from the long fiber retention data for each of these fibers studied in vivo. For those fibers containing less than about 10% by weight of alumina, and for the refractory ceramic fiber, the in-vivo $k_{dis}$ agreed reasonably well with the value measured in vitro. But for the high alumina rock wool compositions containing more than about 10% alumina, it was not possible to measure the dissolution rate in-vitro (Eastes et al., 2000b). The in-vivo $k_{dis}$ will be used consistently in what follows.

The data on each fiber available are summarized in Tables 2 and 3. The fiber compositions that are generally classified as slag or rock wool fibers, both the conventional low alumina and the newer high alumina rock wools, are summarized in Table 2. Table 3 shows the same information for all of the other fiber types, most of which are glass wools, but it also includes refractory ceramic fibers and thin, special purpose E glass fibers. In each table, the fibers are grouped according to the published biopersistence study. Since the composition of each fiber has been previously published as noted in Table 1, it will not be repeated here, but rather the partial dissolution rate $S$ from Eq (3) is given along with the $Al_2O_3/SiO_2$ ratio and the in-vivo $k_{dis}$. However, the complete set of fiber compositions and in-vivo dissolution rates used in this paper are available separately as a tab delimited text file by clicking here.

---

**Table 2.** In-vivo dissolution rate constant $k_{dis}$ in ng/cm$^2$/hr and parameters of the composition for the rock and slag wool fibers.

| Fiber | $k_{dis}$ | gsd[a] | $Al_2O_3/SiO_2$[b] | $S$[c] |
|---|---|---|---|---|
| QFHA 19 | 974 | 1.057 | 0.471 | -0.0271 |
| QFHA 22 | 406 | 1.278 | 0.519 | -0.0201 |
| QFHA 23 | 495 | 1.183 | 0.555 | -0.0266 |
| QFHA 25 | 337 | 1.110 | 0.594 | -0.0349 |
| Rock MMVF 21 | 20 | 1.022 | 0.281 | -0.0477 |
| HT MMVF 34 | 346 | 1.068 | 0.600 | -0.0232 |
| SG F | 180 | 1.331 | 0.056 | -0.0330 |
| SG G | 175 | 1.347 | 0.007 | -0.0266 |
| SG H | 126 | 1.649 | 0.068 | -0.0361 |
| SG L | 26 | 1.974 | 0.291 | -0.0455 |
| Rock Wool MMVF 21 | 25 | 1.042 | 0.281 | -0.0459 |
| | | | | |

| | | | | |
|---|---|---|---|---|
| Slag Wool MMVF 22 | 171 | 1.563 | 0.276 | -0.0868 |

[a] Geometric standard deviation of $k_{dis}$
[b] Weight Ratio
[c] Partial dissolution rate defined by Eq (3)

---

**Table 3.** In-vivo dissolution rate constant $k_{dis}$ in ng/cm$^2$/hr and parameters of the composition for glass wool and refractory ceramic fibers. The footnotes refer to Table 1.

| Fiber | $k_{dis}$ | gsd[a] | $Al_2O_3/SiO_2$[b] | $S$[c] |
|---|---|---|---|---|
| KI-40 | 1198 | 2.923 | 0.038 | -0.0359 |
| NK 8340 | 445 | 1.251 | 0.033 | -0.0130 |
| RCF 1a | 16 | 1.078 | 0.888 | 0.0224 |
| E MMVF 32 | 11 | 1.028 | 0.256 | -0.0480 |
| JM475 MMVF 33 | 17 | 2.549 | 0.102 | -0.0286 |
| SG MMVF 11 | 138 | 1.512 | 0.061 | -0.0191 |
| SG A | 225 | 1.514 | 0.029 | -0.0162 |
| SG B | 989 | 4.655 | 0.005 | -0.0171 |
| SG C | 616 | 2.024 | 0.016 | -0.0211 |
| SG J X607 | 222 | 1.718 | 0.021 | -0.0333 |
| JM 901 MMVF 10 | 36 | 1.419 | 0.091 | -0.0449 |
| CT B MMVF 11 | 133 | 1.245 | 0.061 | -0.0193 |
| 7779 | 3 | 2.614 | 0.135 | -0.0468 |
| 7484 | 124 | 1.227 | 0.063 | -0.0245 |
| 7753 | 244 | 1.309 | 0.008 | -0.0202 |
| MMVF 10 | 201 | 1.316 | 0.091 | -0.0321 |
| MMVF 11 | 96 | 1.170 | 0.060 | -0.0214 |

The partial dissolution rate $S$ is plotted for each fiber as a function of the $Al_2O_3/SiO_2$ ratio in Figure 1. It may be seen from Figure 1 that the partial dissolution rate $S$ is indeed approximately linear in the alumina/silica ratio as suggested by Eq (3) and that there are two distinct regions of linearity, one corresponding to low alumina, and the other to high alumina. Straight lines were fit in the sense of minimum $\chi^2$ to the data in each region. The $R^2$

statistics were 0.969 and 0.957 for the left and right hand lines in Figure 1, respectively.

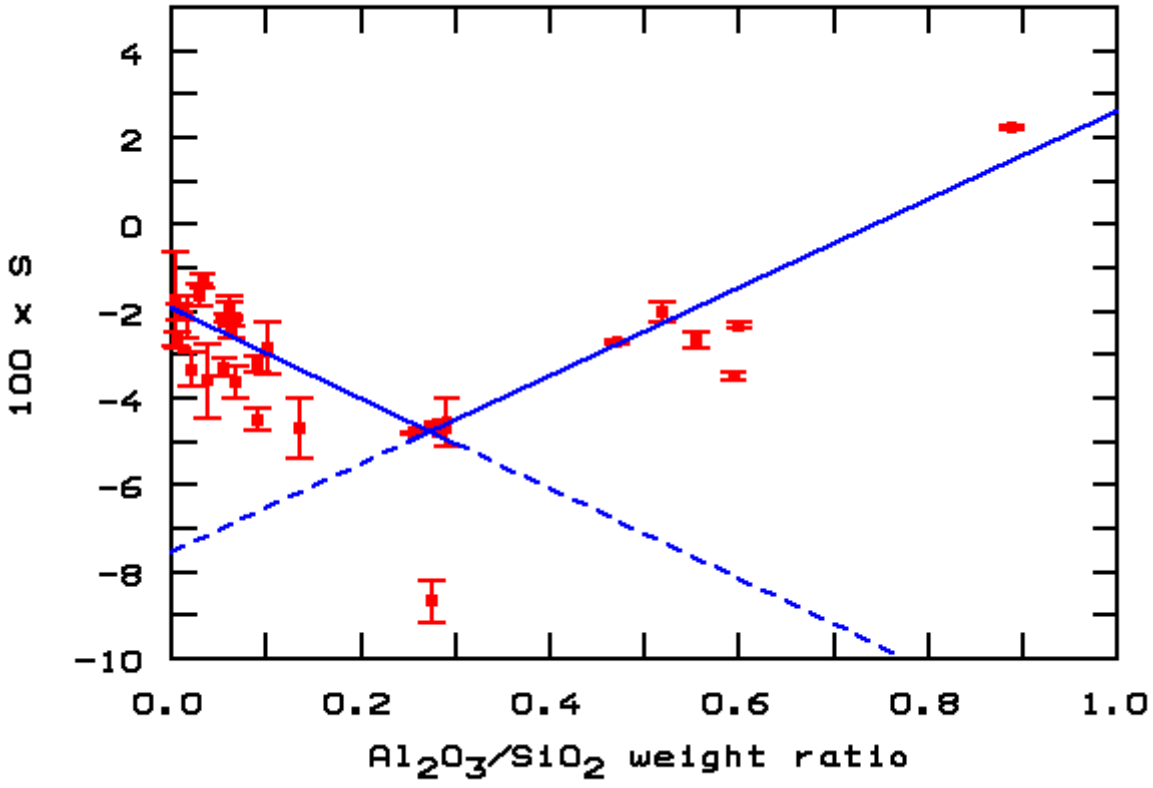


**Figure 1.** Partial dissolution rate *S* derived from in-vivo $k_{dis}$ for the available fibers as a function of the alumina/silica ratio. The vertical bars represent the geometric standard deviation of *S* derived from that of the in-vivo $k_{dis}$.

---

The fiber compositions and in-vivo dissolution rate data shown in Figure 1 were then fit to Eq (4), which includes FeO in the fit. The fit was done twice, once with the low alumina compositions having alumina/silica ratios below 0.30 on the left side of Figure 1, and again with the high alumina compositions with alumina/silica above 0.25. Several compositions where the lines cross in Figure 1 were included in both the low and high alumina fits, as they appear to fit in either category. Two separate sets of coefficients $P_i$ for $SiO_2$, $Al_2O_3$, and FeO were determined, one for the low alumina and one for the high alumina regions. These coefficients are summarized in Table 4 along with the coefficients for the other oxides, which are the same as for the borosilicate fibers by this theory. For comparison, that set of borosilicate coefficients is also shown in Table 4.

Also shown in Table 4 are two statistics of the correlation between the calculated $k_{dis}$ and the in-vivo measured values upon which these coefficients were based. The $R^2$ statistic, which is a measure of the correlation between the calculated and the measured values, may be interpreted as the fraction of the variation in the measured data that is explained by the calculated values. The geometric standard error GSE of the fit to the in-vivo $k_{dis}$ is also given. It may be interpreted as follows: Approximately two-thirds of the calculated $k_{dis}$ values fall within the in-vivo measured value divided by the GSE and the measured value times the GSE. The geometric standard error is the appropriate statistic here rather than the standard error, since the logarithm of $k_{dis}$ was the quantity subjected to a linear fit in Eq (4).

The coefficients in Table 4, when used in Eq (1), provide an estimate of the dissolution rate $k_{dis}$ for a fiber of known composition. This calculation is carried out by first normalizing the oxide composition to 100% in all of the oxides that have coefficients in Table 4. Then, each oxide weight percent is multiplied by the corresponding

coefficient from Table 4 and these are summed. This sum is the logarithm to the base 10 of the dissolution rate, the antilogarithm of which yields the dissolution rate constant in ng/cm$^2$/hr. A computer program that runs in a web page is available to perform this calculation conveniently. The program may be started by clicking here. In practice, it is not necessary to determine beforehand whether a given composition is a low or high alumina composition to know which of the two sets of coefficients in Table 4 apply. One simply calculates $k_{dis}$ by both sets of coefficients, which corresponds to evaluating S on both the solid line and on the dashed line in Figure 1. It is apparent from Figure 1 that the larger value of $S$ and therefore the larger value of $k_{dis}$ so obtained is the correct estimate, because the larger value of $S$ is the one upon which the measured data fall. The computer program just mentioned makes use of these facts to provide an estimate of the dissolution rate of a wide variety of different compositions, using the best set of coefficients for each composition given. The results of applying Eq (1) with the coefficients in Table 4 and the considerations just described to the data of Tables 3 and 4 are summarized in Figure 2 by plotting the in-vivo measured $k_{dis}$ against the calculated value for each fiber. The straight line in Figure 2 is the line on which all of the data would fall if there were perfect agreement of the calculated with the in-vivo measured $k_{dis}$.

---

**Table 4.** Coefficients $P_i$ in Eq (3) for the calculation of $k_{dis}$ from composition for the three types of fibers, shown with the standard error of each coefficient estimated from the fit and statistics of the correlation between the calculated and the measured $k_{dis}$.

| Oxide | Low Alumina | High Alumina | Borosilicate |
|---|---|---|---|
| $SiO_2$ | -0.01711 ± 0.00062 | -0.07423 ± 0.00034 | -0.01198 ± 0.00285 |
| $Al_2O_3$ | -0.12091 ± 0.00262 | 0.10454 ± 0.00088 | -0.21410 ± 0.01102 |
| CaO | 0.10806 ± 0.01119 | 0.10806 ± 0.01119 | 0.10806 ± 0.01119 |
| MgO | 0.13761 ± 0.01262 | 0.13761 ± 0.01262 | 0.13761 ± 0.01262 |
| $Na_2O$ | 0.09386 ± 0.00867 | 0.09386 ± 0.00867 | 0.09386 ± 0.00867 |
| $B_2O_3$ | 0.14669 ± 0.00908 | 0.14669 ± 0.00908 | 0.14669 ± 0.00908 |
| BaO | 0.06921 ± 0.03095 | 0.06921 ± 0.03095 | 0.06921 ± 0.03095 |
| F | 0.11867 ± 0.06134 | 0.11867 ± 0.06134 | 0.11867 ± 0.06134 |
| FeO | 0.05154 ± 0.00303 | -0.01724 ± 0.00244 | - |
| $R^2$ | 0.96 | 0.98 | 0.96 |
| GSE | 3.9 | 4.5 | 1.25 |

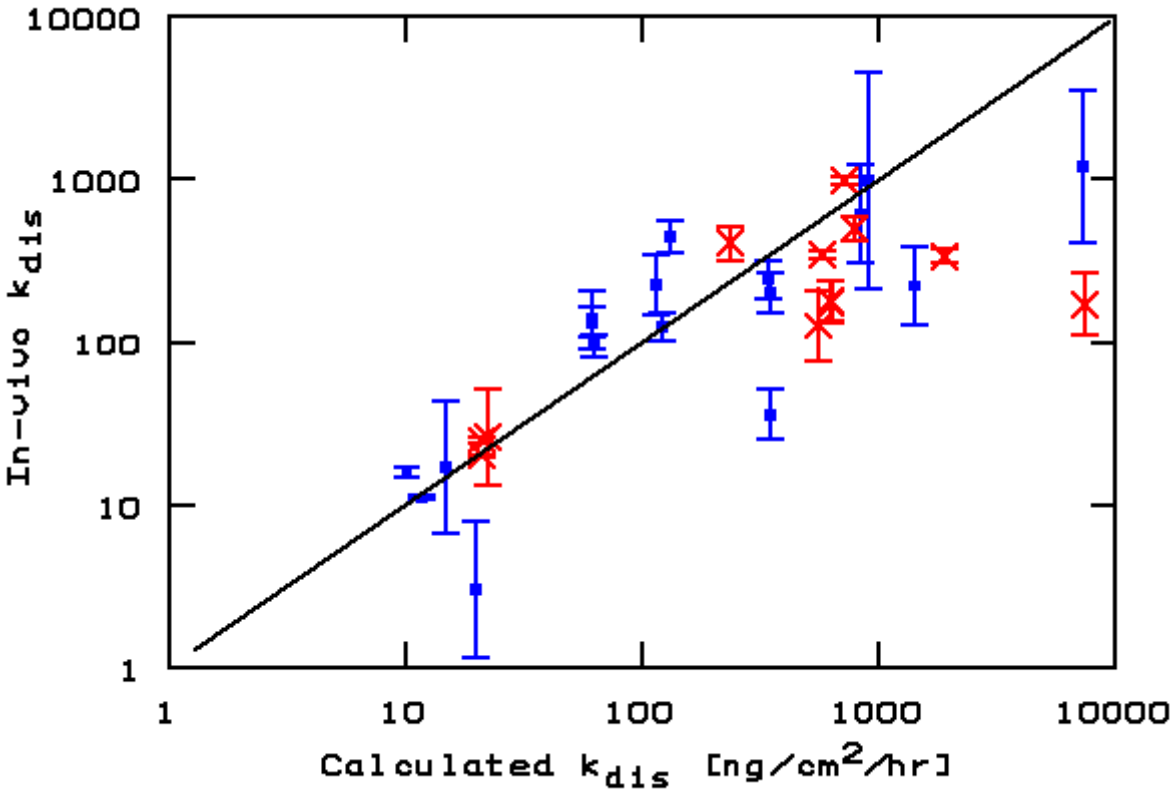


**Figure 2.** Comparison of the dissolution rate constant calculated from the composition with the in-vivo measured value for the data used to determine three of the coefficients. The rock and slag wool compositions from Table 2 are denoted with red **X** symbols, whereas the other compositions from Table 3 are shown with a small blue square. The vertical error bars denote the geometric standard deviation of the in-vivo measured $k_{dis}$.

---

## DISCUSSION

The work described here began as an attempt to extend to rock and slag wool fibers the ability to estimate the dissolution rate constant from composition in the same way as had been done earlier for borosilicate glass fibers (Eastes et al., 2000a). To accomplish this goal, it was necessary to use different equations for the high alumina fiber compositions than for the low alumina fibers. The form of these two equations is the same, but the coefficients are different. Once this division was made, it was found that a much wider variety of fiber compositions, including refractory ceramic fibers and special purpose thin E glass fibers, for example, could be estimated just as well as the rock and slag wool fibers by the same equations. Even borosilicate glass fibers were estimated fairly accurately by the low alumina equation and are included in the results in Figures 1 and 2. Thus the low alumina and the high alumina equation coefficients listed in Table 4 represent a "universal" method for estimating the dissolution rate of a wide variety of commercial and experimental vitreous silicate glass fibers. The low alumina equations work fairly well for the borosilicate glass fibers too, but the borosilicate coefficients provide a much more accurate estimate for those fibers that fall into that class of compositions. For fibers that are not borosilicates, one falls back upon the low or high alumina coefficients, which cover a much wider range of compositions, but with less confidence in the accuracy of the estimate.

As shown in Table 4, all three sets of coefficients have large and similar values of $R^2$, all over 0.95. This fact means that over 95% of the variation in the in-vivo $k_{dis}$ was explained by the calculated values. The real differences among these sets of coefficients is revealed by the geometric standard error of the fit, GSE, which is much smaller for the borosilicate coefficients than for the other two sets. If the composition is a borosilicate, then

one can use these coefficients with the expectation that the calculated value will be within the GSE factor of 1.25 of the actual value about two-thirds of the time. On the other hand, the other two equations are accurate only to a factor of about four in the same sense.

This large difference in the accuracy of the equations comes about because the borosilicate equation was developed over a relatively small range of composition using much more measured data. The low and high alumina coefficients were based on in-vivo data alone on a much smaller set of compositions that at the same time covered a much wider range of composition. The tradeoff between accuracy and composition range covered is a general feature of this sort of dissolution rate model. It is likely that equations could be developed for rock and slag wool that could be just as accurate as the borosilicate equations, if the composition range were just as restricted and the data were available.

Another difference between the borosilicate equation and the other two is that the borosilicate coefficients were developed from in-vitro measured $k_{dis}$, whereas the low and high alumina coefficients were developed exclusively from in-vivo dissolution rates. In nearly all cases, the in-vitro dissolution rates for the low alumina compositions agreed well with in-vivo values (Eastes et al., 2000b), but not for some high alumina fibers. Also, the borosilicate in-vitro $k_{dis}$ measurements agreed well with the in-vivo values that were available. Therefore, the $k_{dis}$ estimates provided by the coefficients in Table 4 may be considered to be estimates of the dissolution rates in vivo, which do in fact agree with the in-vitro $k_{dis}$ for all except the high alumina rock wool compositions.

Figure 2 summarizes the quality of the estimate of dissolution rate provided by the low and high alumina equations by comparing the calculations with the values measured in vivo. It is seen first of all that the calculated values for rock and slag wool compositions are not consistently better or worse than those for borosilicate and other compositions, which underscores the "universal" nature of these equations. However, the quality of the calculated values appears to fall into two distinct regions: Below about 1000 ng/cm$^2$/hr, the calculated $k_{dis}$ agrees reasonably well with the in-vivo value with two notable exceptions; Above 1000, the calculated $k_{dis}$ is typically significantly higher than the in-vivo value.

The two notable exceptions to the reasonable agreement between the calculated and the in-vivo $k_{dis}$ below 1000 ng/cm$^2$/hr in Figure 2 are the fiber 7779 with a calculated $k_{dis}$ of 20 but in-vivo $k_{dis}$ of 3 and JM 901 MMVF 10 with calculated $k_{dis}$ 346 but in vivo $k_{dis}$ 36. In view of the large uncertainty in the in-vivo $k_{dis}$ for 7779, it is not clear that the discrepancy is statistically unexpected. However, the JM 901 MMVF 10 point is an obvious anomaly, differing by almost a factor of ten. It is interesting that the MMVF 10 composition was measured twice in vivo, once by inhalation biopersistence, and again from intratracheal diameter change, and both appear in Figure 2. This latter in-vivo $k_{dis}$ was 201, which agrees with the calculated value within the average error of the calculation. This is the only example known in which two in-vivo tests give such differing results. The weight of

the evidence suggests that the larger $k_{dis}$ is the correct one for this fiber.

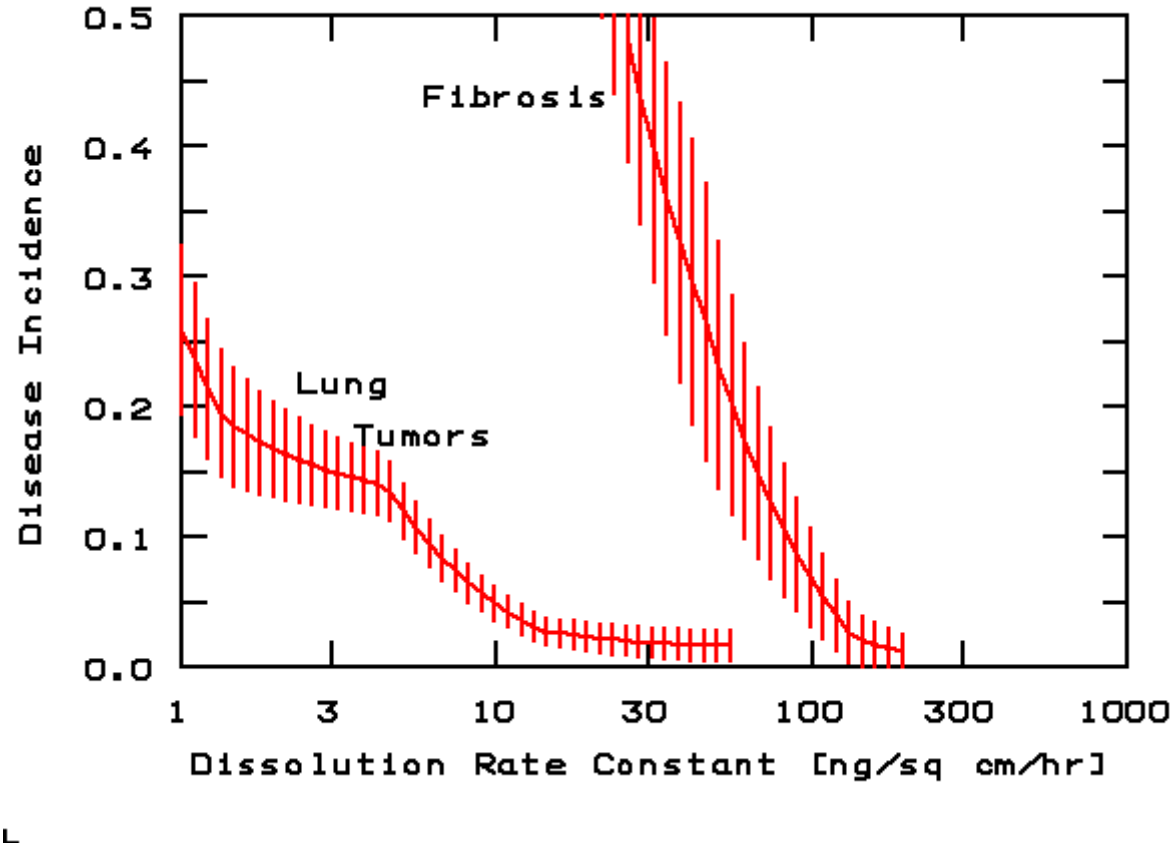


**Figure 3.** Predicted incidence of lung tumors and Wagner Grade 4 or higher fibrosis for chronic inhalation rat studies of 1-$\mu$m-diameter fibers as a function of the fiber dissolution rate constant. The estimated standard error associated with the predicted incidence (solid red lines) are shown as arbitrarily spaced vertical red lines.

---

In the high dissolution region above 1000 ng/cm$^2$/hr, the calculated $k_{dis}$ is consistently larger than the in-vivo measured value. It was noted in a previous study (Eastes et al., 2000b) that the in-vitro measured $k_{dis}$ also appeared to be larger than the in-vivo value, and it was postulated that the nature of the inhalation biopersistence protocol made it difficult to accurately determine the dissolution rate outside the range of 3 to 300 ng/cm$^2$/hr. Not only are such high dissolution rates difficult to determine by inhalation biopersistence, but also they have little significance for chronic effects in rat inhalation studies. Figure 3 (Eastes and Hadley, 1996) shows the incidence of lung tumors and fibrosis predicted in a state of the art chronic rat inhalation study with fibers of different dissolution rates. It is clear from Figure 3 that disease incidence has dropped to background levels at dissolution rates well below the 300 to 1000 ng/cm$^2$/hr at which significant discrepancies are observed between the calculated and either the in-vitro or the in-vivo measured value.

This consideration of the agreement and especially the nature of what lack of agreement exists between the in-vivo and the calculated dissolution rate leads to the seemingly outrageous suggestion that the calculated $k_{dis}$ is more reliable than the measured value, at least for the sorts of fibers studied so far. This unseemly reliability of the calculated $k_{dis}$ could come about because the chemical basis of the calculation method allows it to be extended into regions of high and low dissolution rate where the in-vivo protocol is not as sensitive. In any case, it appears that, when the calculated dissolution rate is very large or very small, then the in-vivo rate is also. It is merely that the quantitative agreement between calculated and in-vivo $k_{dis}$ is not as good as it is in the 3 to 300 ng/cm$^2$/hr region.

The fact that the absolute accuracy of the high alumina and low alumina equations for predicting the in-vivo dissolution rate of rock, slag, and other synthetic vitreous fibers is about a factor of four, as indicated by the geometric standard error (Table 4), needs to be viewed in context. First of all, the range of in-vivo dissolution rate over which this statistic was compiled is about a factor of 400. Thus a method that places the dissolution rate within a factor of four in a range that spans a factor of 400 may have considerable practical utility. Secondly, the in-vivo measured dissolution rate, upon which the calculation methods are verified, are not much more precise either, as seen from the error bars in Figure 2. In fact, five of the 29 fibers exhibited in Tables 2 and 3 have geometric standard deviations for the in-vivo dissolution rate constant above two. Thus the dissolution rate calculated simply from the composition is not a lot less variable than the in-vivo data to which it is being compared.

The method just described provides a way to estimate the dissolution rate constant for a fairly wide range of rock and slag wool and other synthetic vitreous silicate fibers from their compositions. With a knowledge of the dissolution rate constant, one may estimate whether disease would be observed in animal inhalation or intraperitoneal studies, as has been described previously (Eastes and Hadley, 1996). The method given in this paper serves to extend to a wide variety of fiber compositions what has been published previously for borosilicate glass wool fiber types (Eastes et al., 2000a). A computer program that runs in a web page is available to perform this calculation conveniently for any composition entered into it. The program may be started by clicking here.

The ability to determine $k_{dis}$ simply from the composition of a synthetic vitreous silicate fiber should be useful both to fiber manufacturers and to researchers who are interested in changing the dissolution rate of vitreous silicate fibers. Additionally, it provides a tool by which interested regulatory bodies may monitor the dissolution rate of insulation wool products simply by monitoring their composition without expensive and time-consuming animal tests.

**REFERENCES**

Bauer, J., Mattson, S. M., and Eastes W. 1997. In-vitro acellular method for determining fiber durability in simulated lung fluid. Available from the authors.
Read this paper or Download it (24 kB).

Bernstein, D. M., Morscheidt, C., Grimm, H.-G., Thévenaz, P., and Teichert, U. 1996. Evaluation of soluble fibers using the inhalation biopersistence model, a nine-fiber comparison. *Inhal. Toxicol.* 8:345-385.

Eastes, W., Potter, R. M., and Hadley, J. G. 2000a. Estimating in-vitro glass fiber dissolution rate from composition. *Inhal. Toxicol.,* 12:269-280.
Read this paper or Download it (23 kB).

Eastes, W., Potter, R. M., and Hadley, J. G. 2000b. Estimation of dissolution rate from in-vivo studies of synthetic vitreous fibers. *Inhal. Toxicol.,* in press.
Read this paper or Download it (31 kB).

Eastes, W., and Hadley, J. G. 1996. A mathematical model of fiber carcinogenicity and fibrosis in inhalation and intraperitoneal experiments in rats. *Inhal. Toxicol.* 8:323-343.
Read this paper or Download it (60 kB).

Eastes, W., Morris, K. J., Morgan, A., Launder, K. A., Collier, C. G., Davis, J. A., Mattson, S. M., and Hadley, J. G. 1995. Dissolution of glass fibers in the rat lung following intratracheal instillation. *Inhal. Toxicol.* 7:197-213.
Read this paper or Download it (57 kB).

Eastes, W., and Hadley, J. G. 1995. Dissolution of fibers inhaled by rats. *Inhal. Toxicol.* 7:179-196.

Hesterberg, T. W., Chase, G., Axten, C., Miiller, W. C., Musselman, R. P., Kamstrup, O., Hadley, J., Morscheidt, C., Bernstein, D. M., Thévenaz, P. 1998. Biopersistence of synthetic vitreous fibers and amosite asbestos in the

rat lung following inhalation. *Toxicol. and Applied Pharm*. 151:262-275.

Mattson, S. 1994. Glass fibers in simulated lung fluid: Dissolution behavior and analytical requirements. *Ann. occup. Hyg*. 38:857-879.

Musselman, R. P., Miiller, W. C., Eastes, W., Hadley, J. G., Kamstrup, O., Thévenaz, P., Hesterberg, T. W. 1994. Biopersistences of man-made vitreous fibers and crocidolite fibers in rat lungs following short-term exposures *Environ. Health Perspect*. 102(Suppl. 5):139-143.

Potter, R. M. and Mattson, S. M. 1991. Glass fiber dissolution in a physiological saline solution. *Glastech. Ber.* 64:16-28.

Scholze, H. 1988. Durability investigations on siliceous man-made mineral fibers, a critical review. *Glastech. Ber.* 61:161-171.

---

First Page || Next Page